

# Synthesis of MIL-101@g-C<sub>3</sub>N<sub>4</sub> nanocomposite for enhanced adsorption capacity towards CO<sub>2</sub>

Asmaa Argoub<sup>1</sup> · Rachid Ghezini<sup>1</sup> · Cherifa Bachir<sup>1,2</sup> · Bouhadjar Boukoussa<sup>1,3</sup> · Amine Khelifa<sup>4</sup> · Abdelkader Bengueddach<sup>1</sup> · Peter G. Weidler<sup>5</sup> · Rachida Hamacha<sup>1</sup>

**Abstract** MIL-101@g-C<sub>3</sub>N<sub>4</sub> nanocomposite was prepared by solvothermal synthesis and used for CO<sub>2</sub> adsorption. The parent materials (MIL-101 and g-C<sub>3</sub>N<sub>4</sub>) and the MIL-101@g-C<sub>3</sub>N<sub>4</sub> were characterized by X-ray diffraction, argon adsorption/desorption, Fourier transform infrared spectroscopy, thermal analysis (TG/DTA), transmission electronic microscopy, and Energy-dispersive X-ray spectroscopy. The results confirmed the formation of well-defined MIL-101@g-C<sub>3</sub>N<sub>4</sub> with interesting surface area and pore volume. Furthermore, both MIL-101 and MIL-101@g-C<sub>3</sub>N<sub>4</sub> were accomplished in carbon dioxide capture at different temperatures (280, 288, 273 and 298 K)

at lower pressure. The adsorption isotherms show that the nanocomposite has a good CO<sub>2</sub> adsorption affinity compared to MIL-101. The best adsorption capacity is about 1.6 mmol g<sup>-1</sup> obtained for the nanocomposite material which is two times higher than that of MIL-101, indicating strong interactions between CO<sub>2</sub> and MIL-101@g-C<sub>3</sub>N<sub>4</sub>. This difference in efficacy is mainly due to the presence of the amine groups dispersed in the nanocomposite. Finally, we have developed a simple route for the preparation of an effective and new adsorbent for the removal of CO<sub>2</sub>, which can be used as an excellent candidate for gas storage, catalysis, and adsorption.

**Keywords** MIL-101 · Carbon nitride · MIL-101@g-C<sub>3</sub>N<sub>4</sub> nanocomposite · CO<sub>2</sub> adsorption · Adsorption isotherms

✉ Bouhadjar Boukoussa  
bbouhdjer@yahoo.fr

✉ Rachida Hamacha  
hamacha.rachida@univ-oran.dz

<sup>1</sup> Laboratoire de Chimie des Matériaux L.C.M., Université d'Oran1 Ahmed Ben Bella, BP 1524 El-Mnaouer, 31000 Oran, Algeria

<sup>2</sup> Laboratoire de Chimie Appliquée LAC, C.U. Aïn-Témouchent, Route Sidi Bel Abbes BP 284, 46000 Aïn Témouchent, Algeria

<sup>3</sup> Département de Génie des Matériaux, Faculté de Chimie, Université des Sciences et de la Technologie Mohamed Boudiaf, BP 1505 El-Mnaouer, 3100 Oran, Algeria

<sup>4</sup> Laboratoire de Structure, Elaboration et Applications des Matériaux Moléculaires (SEA2M), Université Abdelhamid Ibn Badis Mostaganem, Mostaganem, Algeria

<sup>5</sup> Institute of Functional Interfaces, Karlsruher Institut für Technologie KIT, Hermann-von-Helmholtz-Platz 1, 76344 Eggenstein-Leopoldshafen, Germany

## 1 Introduction

The metal organic frameworks (MOF's) are a new generation of porous materials which can be straightforwardly constructed by the self-assembly of metal ions and/or metal-containing clusters with appropriate organic linkers [1]. Their key factor is related to their high surface area ( $S_{\text{BET}}$ ) and pore size which are considerably larger than those of mesoporous and microporous materials (case of MCM-41, SBA-15, zeolites) [2, 3]. Due to these properties, the MOF's have been extensively investigated in different fields such as gas storage, catalysis, separation, and adsorption [4]. Among the most famous MOF's, there is MIL-101 (Material of Institute Lavoisier n°101) that has drawn much attention due to its high stability compared with other metal-organic frameworks [5]. MIL-101 was first synthesized by Férey et al. in 2005 and has been widely applied in adsorption [6]. This

material has a mesoporous zeotype architecture, with a cubic structure (unit cell parameter  $a \sim 89 \text{ \AA}$ , cell volume of  $70200 \text{ \AA}^3$ ), and pores size close to  $3.4 \text{ nm}$ . All these properties expand the application field of MOF's especially in the gas adsorption [7]. However, due to low density of atoms in the structure, the MOFs cannot provide strong force to efficiently adsorb the gas molecules under ambient pressure [8].

For these reasons, several attempts have been developed to solve these issues by either the modification of the framework itself in the synthesis process [9], or the metal motifs could be integrated into crystalline metal organic framework [10, 11]. Recently, new strategies have been focused on the incorporation of active species into the MIL-101 frameworks [12]. Lin et al. [13] have immobilized polyamine into the MIL-101(Cr) pores; they have demonstrated that this adsorbent displays higher selectivity towards  $\text{CO}_2$  adsorption (using mixture of gas  $\text{CO}_2/\text{N}_2$  and  $\text{CO}_2/\text{CH}_4$ ) compared to that of MIL-101(Cr). The graphene oxide (GrO) has been used for the synthesis of composite GrO@MIL-101 [13]. It possessed higher specific surface area with the larger total pore volume compared to its parent MIL-101(Cr). This new composite material has an excellent adsorption performance for some gases such as  $\text{CO}_2$  and  $\text{CH}_4$ , and also for the  $\text{CO}_2/\text{CH}_4$  separation.

Carbon nitride ( $\text{g-C}_3\text{N}_4$ ) has attracted an intense interest due to its particular electrical and optical properties. It constitutes a useful raw material for improving the mechanical and thermal properties of resulting products [14–16].  $\text{g-C}_3\text{N}_4$  has been used in several fields such as biosensor [17, 18], electrochemical agent [19, 20], catalyst support [21], photocatalysts [22], and sorbent material [23]. The application of the carbon nitride in  $\text{CO}_2$  adsorption showed that this material has a high affinity towards  $\text{CO}_2$  molecules due to the strong acid/base interactions between terminal amines in the  $\text{g-C}_3\text{N}_4$  framework and the  $\text{CO}_2$  acid molecules [24, 25].

By reviewing the previous works in the nanocomposite synthesis, the use of  $\text{g-C}_3\text{N}_4$  in the synthesis of MIL-101@ $\text{g-C}_3\text{N}_4$  composite materials has not yet been investigated so far. So, it is interesting to combine the advantages of both MIL-101 and carbon nitride materials to gain new insights that can be useful for applications in catalysis, sensors, environmental protection and especially in gas adsorption, even though a large number of composites based on MOF's is known [26].

This work focuses on the synthesis, characterization, and application of MIL-101@ $\text{g-C}_3\text{N}_4$  nanocomposite in  $\text{CO}_2$  adsorption as a new contribution for this class of materials. Adsorption properties were measured by the static volumetric method at temperatures 280, 288, 273, and 298 K.

## 2 Experimental

### 2.1 Synthesis of materials

The MIL-101 was prepared according the procedure described by Kim et al. [27]. A mixture of chromium(III) nitrate non hydrated and  $\text{H}_2\text{BDC}$  was placed in a Teflon-lined autoclave filled with water and HF additive. Heating the autoclave in a convection oven at  $490 \text{ K}$  for  $8 \text{ h}$  produced dark green and weakly agglomerated MIL-101. The synthesis of the  $\text{g-C}_3\text{N}_4$  material was carried out by directly heating the melamine at  $823 \text{ K}$  with a heating rate of  $293 \text{ K min}^{-1}$  during  $2 \text{ h}$  [28]. MIL-101@ $\text{g-C}_3\text{N}_4$  nanocomposite was synthesized via solvothermal method using  $0.02 \text{ g}$  of  $\text{g-C}_3\text{N}_4$  mixed with a solution containing a molar composition of  $1 \text{ Cr}(\text{NO}_3)_3 \cdot 9 \text{ H}_2\text{O} : 1 \text{ H}_2\text{BDC} : 0.3 \text{ HF} : 266 \text{ H}_2\text{O}$ . The resulting suspension was transferred to a Teflon-lined steel autoclave and heated at  $293 \text{ K}$  for  $8 \text{ h}$  in a convection oven. The obtained green colored product was then filtered through  $100 \text{ }\mu\text{m}$  sieves to remove the crystalline terephthalic acid ( $\text{H}_2\text{BDC}$ ) in excess and through  $25 \text{ }\mu\text{m}$  filter paper to separate the composite. Thereafter, the separated product was washed 2–3 times with deionized water, followed by a series of purifications: soaking in water at  $343 \text{ K}$  for  $12 \text{ h}$  in hot ethanol at  $353 \text{ K}$  for  $24 \text{ h}$ , and in hot water at  $333 \text{ K}$  for  $12 \text{ h}$ . Finally, the purified product was dried under vacuum at  $423 \text{ K}$  for  $12 \text{ h}$  after filtration. The prepared sample was designated as MIL-101@ $\text{g-C}_3\text{N}_4$ .

### 2.2 Characterization

The crystalline structure of the obtained materials was determined by X-ray diffraction (XRD) using a Bruker AXS D8 Advance diffractometer working with  $\text{CuK}\alpha$  radiation ( $\lambda = 1.5418 \text{ \AA}$ ) equipped with a Lynxeye Trade Mark(TM) position sensitive stripe detector. Diffractograms were recorded over the range  $2\theta = 0.5^\circ - 30^\circ$  (step size  $2\theta = 0.02^\circ$ , step time  $4 \text{ s}$ ) for both MIL-101 and nanocomposite and over the range  $2\theta = 4^\circ - 60^\circ$  (step size  $2\theta = 0.02^\circ$ , step time  $4 \text{ s}$ ) for  $\text{g-C}_3\text{N}_4$ . Argon adsorption–desorption measurements were performed at  $87 \text{ K}$  using a Quantachrome Autosorb-1MP instrument in the relative pressure range  $P/P_0$  from  $10^{-5}$  to 1. The samples were outgassed overnight at  $383 \text{ K}$  prior to adsorption analysis. Specific surface areas,  $S_{\text{BET}}$ , were calculated according to the Brunauer–Emmett–Teller (BET) method [29]. The non-local density functional theory (NLDFT) was explored based on the normal DFT method. NLDFT is able to correlate the properties of gas molecules with their adsorption performance in different pore sizes. The NLDFT model is accurate in depicting the fluid approaching the pore walls [30] and getting more reliable size estimation. For the obtained samples, NLDFT was used to calculate the total

pore volume  $V_p$  and average pore diameter ( $D_p$ ) from the adsorption branch. The NLDFT differential pore volume distribution curves of all materials were also illustrated. The Ar adsorption–desorption isotherms have been also established, in order to get information on the forms of the isotherms and their hysteresis loop which are related to the pore nature existing in their structure [31, 32]. The Fourier transform infrared spectroscopy (FT-IR) was operated on a Fourier transforms infrared spectrophotometer alpha bruker platinumium-ATR in the 4000–500  $\text{cm}^{-1}$  region. Thermogravimetry combined with differential thermal analysis (TG/DTA) were performed in air using a LABSYS EVO DTA/DSC-Setaram. The MIL-101@g-C<sub>3</sub>N<sub>4</sub> sample was heated from 283 to 1073 K with a heating rate of 283 K  $\text{min}^{-1}$ .

### 2.3 CO<sub>2</sub> adsorption experiment

The CO<sub>2</sub> adsorption/desorption isotherms were determined by micromeritics ASAP 2020 at 273, 280, 288, and 298 K. All samples were outgassed at 110 °C under vacuum for 12 h before CO<sub>2</sub> (ultra-high purity grade) adsorption. The adsorbed amounts were calculated by the volumetric method at pressure lower than 1 atm.

## 3 Results and discussion

### 3.1 Characterization of the materials

The diffraction patterns of MIL-101, MIL-101@g-C<sub>3</sub>N<sub>4</sub> nanocomposite, and g-C<sub>3</sub>N<sub>4</sub> are shown in Fig. 1a, b. For the case of pure g-C<sub>3</sub>N<sub>4</sub> (Fig. 1a), two distinct peaks were observed at  $2\theta = 13.2^\circ$  and  $27.3^\circ$ . The first one, related to the periodic arrangement of the condensed tris-triazine units in the sheets, is indexed as (001). The intense peak at  $27.3^\circ$  is due to the inter-planar distance of conjugated aromatic heptazine layer system units indexed as (002) [28]. The diffraction pattern of MIL-101(Cr) (Fig. 1b) is similar to that obtained by Férey et al. [6].

For the MIL-101@g-C<sub>3</sub>N<sub>4</sub> composite, the XRD pattern (Fig. 1b) is similar to that of MIL-101 with slight decrease in the peaks intensities, showing that MIL-101 structure is not strongly affected after introduction of low content of carbon nitride.

The chemical composition of MIL-101@g-C<sub>3</sub>N<sub>4</sub> nanocomposite is determined by EDX elemental analysis (Fig. S1), which confirms the presence of g-C<sub>3</sub>N<sub>4</sub> in the nanocomposite structure. The same trends have been observed by Li et al. [33] during the preparation of MIL-101(Cr)/graphene oxide composites. It is known that MIL-101 has octahedron crystals, after modification by g-C<sub>3</sub>N<sub>4</sub>, the morphology of the nanocomposite is maintained as indicated

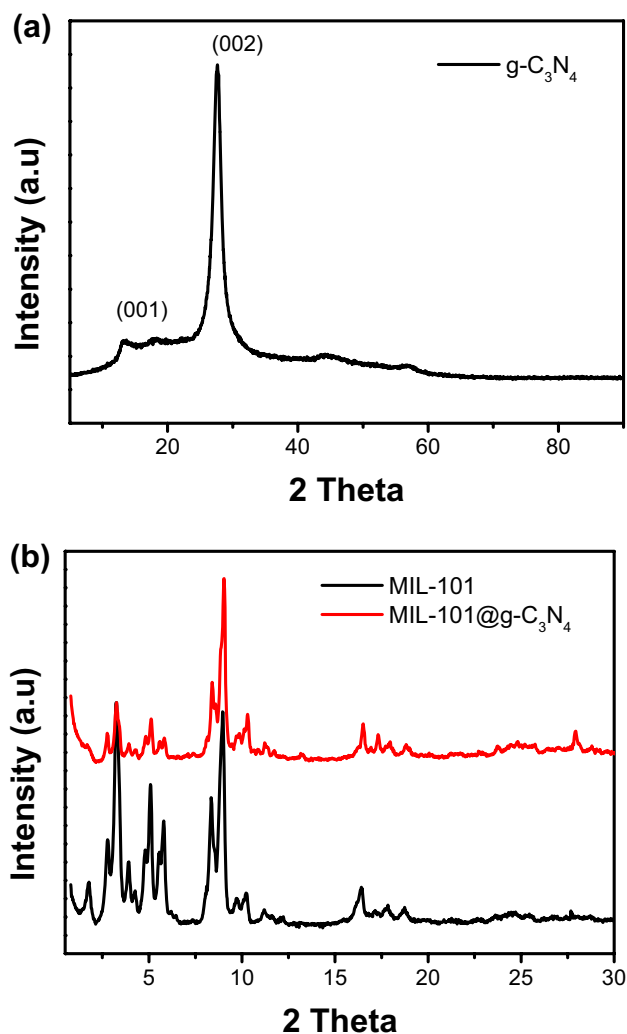
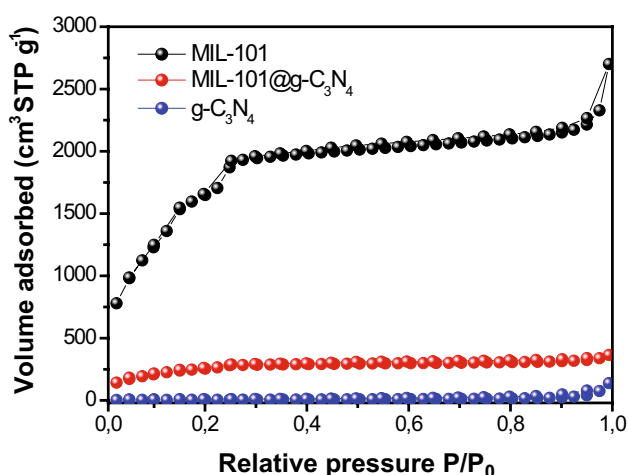


Fig. 1 XRD patterns of the obtained materials

by TEM analysis (Fig. S2). The size of the crystals varies between 80 and 150 nm. No phase of g-C<sub>3</sub>N<sub>4</sub> was detected, showing his good dispersion into the nanocomposite.

Figure 2 shows the argon adsorption–desorption isotherms of the obtained materials. According to the IUPAC classification [29], the adsorption isotherms at 87 K for all samples are mostly of type I, which mainly indicates the presence of micropores. It is also observed that MIL-101 exhibits two secondary uptakes near  $P/P_0 = 0.1$  and  $0.2$ , indicating the presence of two nanoporous windows in the framework. The MIL-101@g-C<sub>3</sub>N<sub>4</sub> nanocomposite shows small indistinct hysteresis loop which is probably related to capillary condensation in large pores in the interparticle space.

Textural parameters including specific surface areas  $S_{\text{BET}}$ , porous volume  $V_p$ , and average pore diameter ( $D_p$ ) of the prepared materials are summarized in Table 1. The MIL-101(Cr) exhibits  $S_{\text{BET}}$  of 4252  $\text{m}^2 \text{g}^{-1}$  and



**Fig. 2** Argon adsorption–desorption isotherms of the obtained materials

**Table 1** Textural parameters of MIL-101 and MIL-101@g-C<sub>3</sub>N<sub>4</sub> nanocomposite

Sample	$S_{\text{BET}}^{\text{a}}$ ( $\text{m}^2 \text{g}^{-1}$ )	$V_{\text{p}}^{\text{b}}$ ( $\text{cm}^3 \text{g}^{-1}$ )	$D_{\text{p}}^{\text{c}}$ (nm)
MIL-101	4252	2.9	2.3
MIL-101@g-C <sub>3</sub> N <sub>4</sub>	837	0.4	2.3

<sup>a</sup>Specific surface area

<sup>b</sup>Pore volume

<sup>c</sup>Pore diameter

$V_{\text{p}} = 2.9 \text{ cm}^3 \text{ g}^{-1}$ . These data are close to previous reported values [6]. Furthermore, the specific surface area as well as the pore volume decreased after g-C<sub>3</sub>N<sub>4</sub> incorporation ( $837 \text{ m}^2 \text{ g}^{-1}$ ,  $0.4 \text{ cm}^3 \text{ g}^{-1}$ ). The reduction of these parameters might be due to an increase in the distortion of the MIL-101 structure owing to the incorporation of g-C<sub>3</sub>N<sub>4</sub>. Moreover, the same value of pore diameter  $D_{\text{p}}$  has been obtained for both materials, it seems that this textural parameter has no direct relationship with the g-C<sub>3</sub>N<sub>4</sub> amount.

The pore size distribution profile was calculated from the adsorption branch of Ar-isotherms as shown in Fig. 3.

It is clearly indicated that the pore size distribution curves of both MIL-101 and MIL-101@g-C<sub>3</sub>N<sub>4</sub> samples are similar (Fig. 3). However, the nanocomposite has a lower pore volume compared to that of MIL-101, due to the filling of the pores by g-C<sub>3</sub>N<sub>4</sub> (Table 1). MIL-101 exhibits two types of pores centred at 1.4 and 2.3 nm. As shown in Fig. 3S, the pore size distribution of the g-C<sub>3</sub>N<sub>4</sub> material indicates small pores diameter.

Therefore, MIL-101@g-C<sub>3</sub>N<sub>4</sub> is in close agreement with the porous structure parameters of both MIL-101 and g-C<sub>3</sub>N<sub>4</sub> samples. This could be ascribed to the assumption

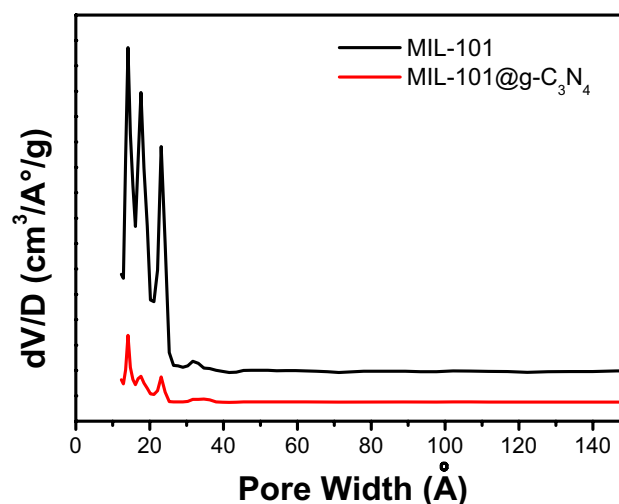


**Fig. 3** Pore size distributions of MIL-101 and MIL-101@g-C<sub>3</sub>N<sub>4</sub>

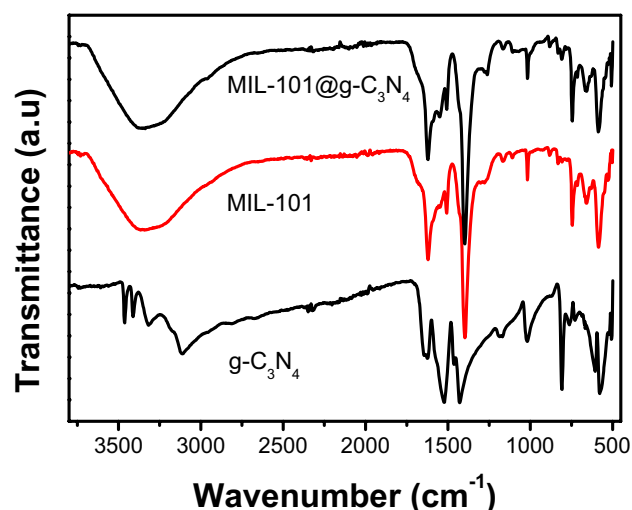


**Fig. 4** FTIR spectra of MIL-101, g-C<sub>3</sub>N<sub>4</sub> and MIL@g-C<sub>3</sub>N<sub>4</sub>

that g-C<sub>3</sub>N<sub>4</sub> provides new crystallization sites into the MIL-101 crystallites.

FTIR spectra of MIL-101, g-C<sub>3</sub>N<sub>4</sub> and MIL-101@g-C<sub>3</sub>N<sub>4</sub> are shown in Fig. 4. In the g-C<sub>3</sub>N<sub>4</sub> spectrum, the band in the range of 1200–1650  $\text{cm}^{-1}$  is assigned to the stretching vibration of heptazine heterocyclic and the sharp band at 800  $\text{cm}^{-1}$  is characteristic either of triazine or heptazine heterocycle units. The broad absorption bands at 3100 and 3400  $\text{cm}^{-1}$  are ascribed to the stretching vibration modes of residual N–H or O–H bands, which are associated with uncondensed amino groups or adsorbed H<sub>2</sub>O molecules [28], respectively. For MIL-101, the bands at 3500 and 1620  $\text{cm}^{-1}$  indicate the presence of adsorbed water. The bands at 1502 and 1404  $\text{cm}^{-1}$  correspond to the O–C–O symmetric vibrations, implying the presence of

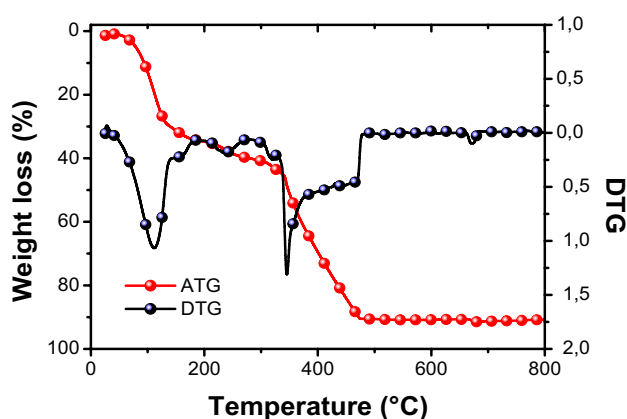


Fig. 5 TG/DTA curves of MIL@g-C<sub>3</sub>N<sub>4</sub>

dicarboxylate within the MIL-101(Cr) framework [6, 34]. The other bands between 600 and 1600 cm<sup>-1</sup> are attributed to benzene, including the stretching of C=C at 1508 cm<sup>-1</sup> and the deformation vibration of C-H at 1107, 940, 760, and 707 cm<sup>-1</sup> [34, 35]. The IR spectrum of the MIL-101@g-C<sub>3</sub>N<sub>4</sub> nanocomposite is similar to that of MIL-101. However, new bands appeared at 586 and 1013 cm<sup>-1</sup>, corresponding to the C-N-C trigonal bending [36].

The TGA curve of the MIL@g-C<sub>3</sub>N<sub>4</sub> nanocomposite is shown in Fig. 5. There is two weight loss steps, the first step occurs in the range 25–150 °C, which is related to the loss of free and bound water molecules. This result is in agreement with FTIR analysis, which proves the existence of water molecules in MIL@g-C<sub>3</sub>N<sub>4</sub>. The second weight loss occurs at 350–375 °C, consequence to the decomposition of the benzenedicarboxylic acid linkers [6, 37]. The DTG curve of MIL@g-C<sub>3</sub>N<sub>4</sub> shows a slight loss at 670 °C, suggesting that some of g-C<sub>3</sub>N<sub>4</sub> species undergo chemical changes [28].

### 3.2 CO<sub>2</sub> adsorption

CO<sub>2</sub> adsorption experiments were carried out on MIL-101 and MIL-101@g-C<sub>3</sub>N<sub>4</sub> at temperatures 273, 280, 288, and 298 K, and at low pressure ( $\approx$ 1 atm). Firstly, we established a comparison between MIL-101 and MIL-101@g-C<sub>3</sub>N<sub>4</sub>, via CO<sub>2</sub> adsorption using the same conditions. Figure 6 shows that the composite material has a better adsorption capacity than MIL-101. This difference is associated with the nature of sites linked on the composite surface. The presence of amines in graphite is the key factor allowing to the composite of attracting CO<sub>2</sub> molecules by acid/base interactions. Our results are consistent with the literature [34, 35]. CO<sub>2</sub> adsorption for both materials decreases gradually with increasing temperature, confirming that the adsorption process takes place via physical interactions [38].

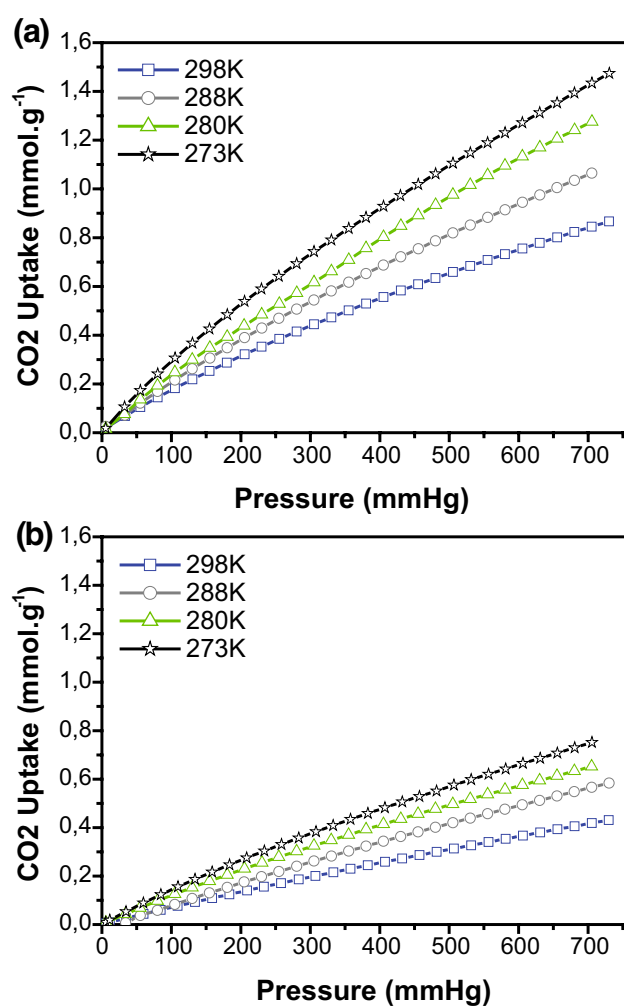


Fig. 6 CO<sub>2</sub> adsorption isotherms. **a** MIL-101@g-C<sub>3</sub>N<sub>4</sub> nanocomposite and **b** MIL-101

As shown in Table 2, our nanocomposite highlights interesting results compared to MIL-101, PEHA-MIL-101, MIL-53, and amino-MIL-53. This is due to the presence of amine groups in the nanocomposite structure, which enhance the interactions with CO<sub>2</sub> acid molecules. Among exceptions, MIL-96 shows the best adsorption capacity probably due to the chemical nature of this product. We also note that MIL-101 prepared in this work has a better CO<sub>2</sub> adsorption capacity compared to that obtained by Anbia and Hoseini [39]. This is strongly due to the large specific surface area and pore volume obtained in this study. We note that the best results have been obtained for amine-modified materials, which result in strong interactions compared to materials containing nanoparticles of metals on the surface. Even if the mesoporous materials are characterized by large surfaces and high pore diameters, without modification these solids have low interactions between the silanol groups and CO<sub>2</sub> molecules [40–46].

**Table 2** Comparison of CO<sub>2</sub> adsorption capacities on different adsorbents

Samples	Pression (bar)	Temperature (K)	CO <sub>2</sub> adsorption method	CO <sub>2</sub> (mmol g <sup>-1</sup> )	Refs.
MIL-101 <sup>a</sup>	10	298	Volumetric	0.85	[39]
PEHA-MIL-101 <sup>b</sup>	10	298	Volumetric	1.30	[39]
MIL-53	1	273	Volumetric	1.45	[47]
MIL-96	1	273	Volumetric	2.81	[47]
amino-MIL-53	1	273	Volumetric	1.09	[47]
Kanemite	1	273	Volumetric	0.05	[38]
PPy/Fe-kan (5%) <sup>c</sup>	1	273	Volumetric	1.70	[38]
SBA <sub>g</sub> -DT <sup>d</sup>	1	318	Thermogravimetric	1.90	[48]
Fe-SBA-15 <sup>e</sup>	//	//	TPD	0.45	[49]
NaMt-MNPs <sup>f</sup>	//	//	TPD	0.65	[50]
MIL-101	1	273	Volumetric	0.75	This work
MIL-101@g-C <sub>3</sub> N <sub>4</sub>	1	273	Volumetric	1.60	This work

<sup>a</sup>MIL-101 prepared from terephthalic acid, Cr(NO<sub>3</sub>)<sub>3</sub>·9H<sub>2</sub>O, HF, H<sub>2</sub>O, S<sub>BET</sub>=1312 m<sup>2</sup> g<sup>-1</sup>, pore volume=1.56 cm<sup>3</sup> g<sup>-1</sup>

<sup>b</sup>MIL-101 modified by pentaethylenehexamine

<sup>c</sup>Nanocomposite containing polypyrrole and kanemite

<sup>d</sup>SBA-15 silica functionalized by grafting with diethylenetriamine (DT)

<sup>e</sup>Fe-SBA-15 incorporation of Fe<sup>0</sup> nanoparticles in the mesoporous channels

<sup>f</sup>Montmorillonite containing the nanoparticle of Pd<sup>0</sup>

## 4 Conclusion

MIL-101@g-C<sub>3</sub>N<sub>4</sub> nanocomposite and MIL-101 were successfully prepared by hydrothermal method and used for CO<sub>2</sub> adsorption. Surface area and pore volume obtained for MIL-101@g-C<sub>3</sub>N<sub>4</sub> are 837 m<sup>2</sup>g<sup>-1</sup> and 0.4 cm<sup>3</sup>g<sup>-1</sup>, respectively. The application of MIL-101@g-C<sub>3</sub>N<sub>4</sub> nanocomposite in adsorption has improved the capacity in CO<sub>2</sub> comparatively to the pure MIL-101, which is mainly due to the presence of strong basic sites containing amine moiety on the surface of nanocomposite. The increase in temperature for the both materials results in the decrease of the adsorption capacity, due to physical interactions between the adsorbent and the adsorbate. A comparison between the MIL-101 and MIL-101@g-C<sub>3</sub>N<sub>4</sub> materials shows that the latter possesses specific interactions with CO<sub>2</sub> molecules through the deep implication of amine moiety anchored in the pores of nanocomposite.

## References

1. T.R. Cook, Y.R. Zheng, P.J. Stang, *Chem. Rev.* **113**(1), 734–777 (2012)
2. H. Yoshitake, T. Yokoi, T. Tatsumi, *Chem. Mater* **14**(11), 4603–4610 (2002)
3. Y. Ma, W. Tong, H. Zhou, S.L. Suib, *Microporous Mesoporous Mater.* **37**(1), 243–252 (2000)
4. S. Kitagawa, *Chem. Soc. Rev.* **43**, 5415 (2014)
5. C. Janiak, J.K. Vieth, *New J. Chem.* **34**(11), 2366–2388 (2010)
6. G. Férey, C. Mellot-Draznieks, C. Serre, F. Millange, J. Dutour, S. Surblé, I. Margiolaki, *Science* **309**(5743), 2040–2042 (2005)
7. P. Chowdhury, S. Mekala, F. Dreisbach, S. Gumma, *Microporous Mesoporous Mater.* **152**, 246–252 (2012)
8. C. Petit, T.J. Bandoz, *Adv. Mater.* **21**, 4753–4757 (2009)
9. Z. Zhang, Y. Zhao, Q. Gong, Z. Li, J. Li, *Chem. Commun.* **49**(7), 653–661 (2013)
10. J. Zhou, K. Liu, C. Kong, L. Chen, *Bull. Korean Chem. Soc.* **34**(6), 1625–1631 (2013)
11. H.G.T Nguyen, M.H. Weston, O.K. Farha, J.T. Hupp, *CrystEngComm* **14**(12), 4115–4118 (2012)
12. Y.K. Hwang, D.Y. Hong, J.S. Chang, S.H. Jung, Y.K. Seo, J. Kim, G. Férey, *Angew. Chem. Int. Ed.* **47**(22), 4144–4148 (2008)
13. Y. Lin, H. Lin, H. Wang, Y. Suo, B. Li, C. Kong, *J. Mater. Chem. A* **2**(35), 14658–14665 (2014)
14. Q. Yan, Y. Lin, C. Kong, L. Chen, *Chem. Commun.* **49**(61), 6873–6875 (2013)
15. X. Zhou, W. Huang, J. Miao, Q. Xia, Z. Zhang, *Chem. Eng. J.* **266**, 339–344 (2015)
16. M. Aono, T. Takeno, T. Takagi, *Diamond Relat. Mater.* **63**, 120–124 (2016)
17. S. Fujita, H. Habuchi, S. Takagi, H. Takikawa, *Diamond Relat. Mater.* **65**, 83–86 (2016)
18. H. Liao, B. Zhang, L. Huang, D. Ma, Z. Jiao, Y. Xie, *Prog. Org. Coat.* **89**, 35–41 (2015)
19. M. Xiong, Q. Rong, H. Meng, X. Zhang, *Biosens. Bioelectron.* **89**, 212–223 (2017)
20. H. Zhang, Y. Huang, S. Hu, Q. Huang, C. Wei, W. Zhang, *Electrochim. Acta* **176**, 28–35 (2015)
21. S. Chen, A. Li, L. Zhang, J. Gong, *Anal. Chim. Acta* **896**, 68–77 (2015)
22. J. Xu, F. Wu, Q. Jiang, J.K. Shang, Y.X. Li, *J. Mol. Catal. A* **403**, 77–83 (2015)

23. H. Li, F.Q. Shao, H. Huang, J.J. Feng, A.J. Wang, *Sens. Actuators B* **226**, 506–511 (2016)
24. G. Mamba, A.K. Mishra, *Appl. Catal. B* **198**, 347–377 (2016)
25. K.S. Lakhi, W.S. Cha, S. Joseph, B.J. Wood, S.S. Aldeyab, *Catal. Today* **243**, 209–217 (2015)
26. Y. Sun, W. Ha, J. Chen, H. Qi, Y. Shi, *Trends Anal. Chem* **84**, 12–21 (2016)
27. J. Kim, Y.R. Lee, W.S. Ahn, *Chem. Commun.* **49**(69), 7647–7649 (2013)
28. S.C. Yan, Z.S. Li, Z.G. Zou, *Langmuir* **25**(17), 10397–10401 (2009)
29. S. Brunauer, P.H. Emmett, E. Teller, *J. Am. Chem. Soc.* **60**, 309–319 (1938)
30. D. Zhao, Y. Wan, W. Zhou, *Structural Characterization Methods* (Wiley-VCH Verlag GmbH & Co. KGaA, Weinheim, 2013). doi:10.1002/9783527647866.ch4
31. K.S.W. Sing, D.H. Everett, R.A.W. Haul, L. Moscou, R.A. Pierotti, J. Rouquérol, T. Siemieniowska, *Pure Appl. Chem.* **57**, 603–619 (1985)
32. M. Eddaoudi, *Characterization of porous solids and powders: surface area, pore size and density*. Particle Technology Series, S. Lowell (Quantachrome Instruments, Boynton Beach), J.E. Shields (CW Post Campus of Long Island University), M.A. Thomas, M. Thommes (Quantachrome Instruments) ed, Dordrecht, The Netherlands, (2005)
33. G. Li, F. Li, H. Yang, F. Cheng, N. Xu, W. Shi, P. Cheng, *Inorg. Chem. Commun.* **64**, 63–66 (2016)
34. X. Zhou, W. Huang, J. Shi, Z. Zhao, Q. Xia, Y. Li, H. Wang, *J. Mater. Chem. A* **2**(13), 4722–4730 (2014)
35. D.Y. Hong, Y.K. Hwang, C. Serre, G. Férey, *Adv. Funct. Mater.* **19**(10), 1537–1552 (2009)
36. X. Sun, Q. Xia, Z. Zhao, Y. Li, Z. Li, *Chem. Eng. J.* **239**, 226–232 (2014)
37. S. H. Jhung, J.-H. Lee, J.W. Yoon, C. Serre, G. Férey, J.S. Chang, *Adv. Mater.* **19**(1), 121–124 (2007)
38. B. Boukoussa, F. Abidallah, Z. Abid, Z. Talha, N. Taybi, H. Sid El Hadj, R. Ghezini, R. Hamacha, A. Bengueddach, *J. Mater. Sci.* **52**, 2460–2472 (2017)
39. M. Anbia, V. Hoseini, *J. Nat. Gas Chem.* **21**, 339–343 (2012)
40. H. Sekkiou, B. Boukoussa, R. Ghezini, Z. Khenchoul, A. Ouali, R. Hamacha, A. Bengueddach, *Mater. Res. Express* **3**(8), 085501 (2016)
41. B. Boukoussa, F. Sebih, R. Hamacha, S. Bellahouel, A. Derdour, A. Bengueddach, *Res. Chem. Intermed.* **41**, 2221–2233 (2015)
42. B. Boukoussa, R. Hamacha, A. Morsli, A. Bengueddach, *Arabian J. Chem.* (2013). doi:10.1016/j.arabjc.2013.07.049
43. K. Chikh, B. Boukoussa, L. Bouhadjar, M. Bencheikh, R. Hamacha, R. Meghabar, M. Belbachir, A. Bengueddach, *Res. Chem. Intermed.* **41**, 6485–6496 (2015)
44. B. Boukoussa, S. Zeghada, G.B. Ababsa, R. Hamacha, A. Derdour, A. Bengueddach, F. Mongin, *Appl. Catal. A* **489**, 131–139 (2015)
45. B. Boukoussa, N. Aouad, R. Hamacha, A. Bengueddach, *J. Phys. Chem. Solids* **78**, 78–83 (2015)
46. I. Terrab, R. Ouargli, B. Boukoussa, K. Ghomari, R. Hamacha, R. Roy, A. Azzouz, A. Bengueddach, *Res. Chem. Intermed.* (2017). doi:10.1007/s11164-016-2846-7
47. H.R. Abid, Z.H. Rada, J. Shang, S. Wang, *Polyhedron* **120**, 103–111 (2016)
48. E.S. Sanz-Pérez, T.C.M. Dantas, A. Arencibia, G. Calleja, A.P.M.A. Guedes, A.S. Araujo, R. Sanz, *Chem. Eng. J.* **308**, 1021–1033 (2017)
49. N. Bouazizi, R. Ouargli, S. Nouisir, R. Benslama, A. Azzouz, *J. Phys. Chem. Solids* **77**, 172–177 (2015)
50. N. Bouazizi, D. Barrimo, S. Nouisir, R.B. Slama, R. Roy, A. Azzouz, *Appl. Surf. Sci.* **402**, 314–322 (2017)

## Repository KITopen

Dies ist ein Postprint/begutachtetes Manuskript.

Empfohlene Zitierung:

Argoub, A.; Ghezini, R.; Bachir, C.; Boukoussa, B.; Khelifa, A.; Bengueddach, A.; Weidler, P. G.; Hamacha, R.

[Synthesis of MIL-101@g-C<sub>3</sub>N<sub>4</sub> nanocomposite for enhanced adsorption capacity towards CO<sub>2</sub>.](#)

2018. Journal of porous materials

[doi:10.5445/IR/1000069473](https://doi.org/10.5445/IR/1000069473)

Zitierung der Originalveröffentlichung:

Argoub, A.; Ghezini, R.; Bachir, C.; Boukoussa, B.; Khelifa, A.; Bengueddach, A.; Weidler, P. G.; Hamacha, R.

[Synthesis of MIL-101@g-C<sub>3</sub>N<sub>4</sub> nanocomposite for enhanced adsorption capacity towards CO<sub>2</sub>.](#)

2018. Journal of porous materials, 25 (1), 199–205.

[doi:10.1007/s10934-017-0433-y](https://doi.org/10.1007/s10934-017-0433-y)